Expanded View Figures

Figure EV1. Myosin VI localisation at the centrosome.

A Total lysates from the indicated cell lines were IB as indicated. No major difference at the level of expression level is visible.

B Expression of myosin VI isoforms in the indicated cell lines was assessed by RT–PCR analysis as previously described (Wollscheid *et al*, 2016). Caco-2 cells grown at confluency express mainly myosin VI long isoform.

C A549 wild-type and myosin VI KO cells were immunostained with anti-myosin VI and anti-pericentrin antibodies. Co-localisation between myosin VI and pericentrin is lost in myosin VI KO cells, as evaluated by Manders' coefficient M2 that measures the fraction of pericentrin overlapping with myosin VI staining. Bars represent mean ± SD. $n = 64$-77 cells from two independent experiments. ****$P < 0.0001$ by Kruskal–Wallis test. Representative images are shown; scale bar, 10 μm. Bottom panel, total lysates from the indicated cell lines were IB as indicated.

D Proximity ligation assay (PLA) in hTERT-RPE1 cells overexpressing GFP-myosin VI_{short} full-length, using anti-OFD1 and anti-GFP antibodies. After PLA assay, counterstaining with fluorescently labelled secondary antibodies allowed the detection of OFD1 and GFP localisation. Left: representative images of technical controls with single or no primary antibodies are shown. Scale bar, 10 μm (2 μm for the magnification). Right: quantification of the percentage of GFP-positive cells that show co-localisation between OFD1 and PLA signal. Bars represent mean ± SD. $n = 3$ independent experiments (46-58 cells/condition).

Source data are available online for this figure.

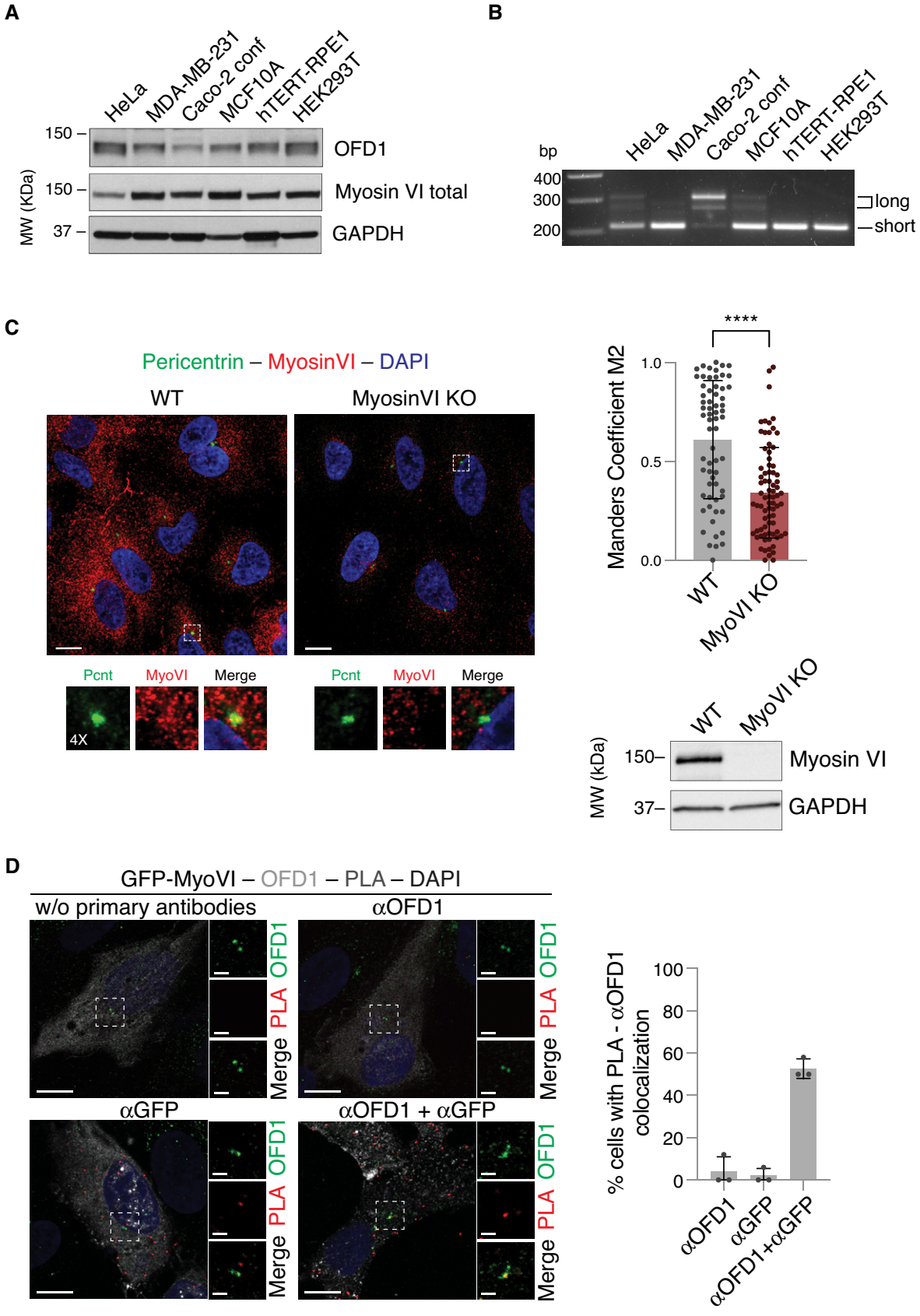
A
HeLa
MDA-MB-231
Caco-2 conf
MCF10A
hTERT-RPE1
HEK293T
150 –
OFD1
MW (KDa)
150 –
Myosin VI total
37 –
GAPDH
B
bp
400
300
200
long
short
C
Pericentrin – MyosinVI – DAPI
WT
MyosinVI KO
Pcnt
MyoVI
Merge
4X
****
Manders Coefficient M2
1.0
0.5
0.0
WT
MyoVI KO
MW (kDa)
150–
Myosin VI
37–
GAPDH
D
GFP-MyoVI – OFD1 – PLA – DAPI
w/o primary antibodies
αOFD1
αGFP
αOFD1 + αGFP
Merge PLA OFD1
% cells with PLA - αOFD1 colocalization
100
80
60
40
20
0
αOFD1
αGFP
αOFD1+αGFP

Figure EV1.

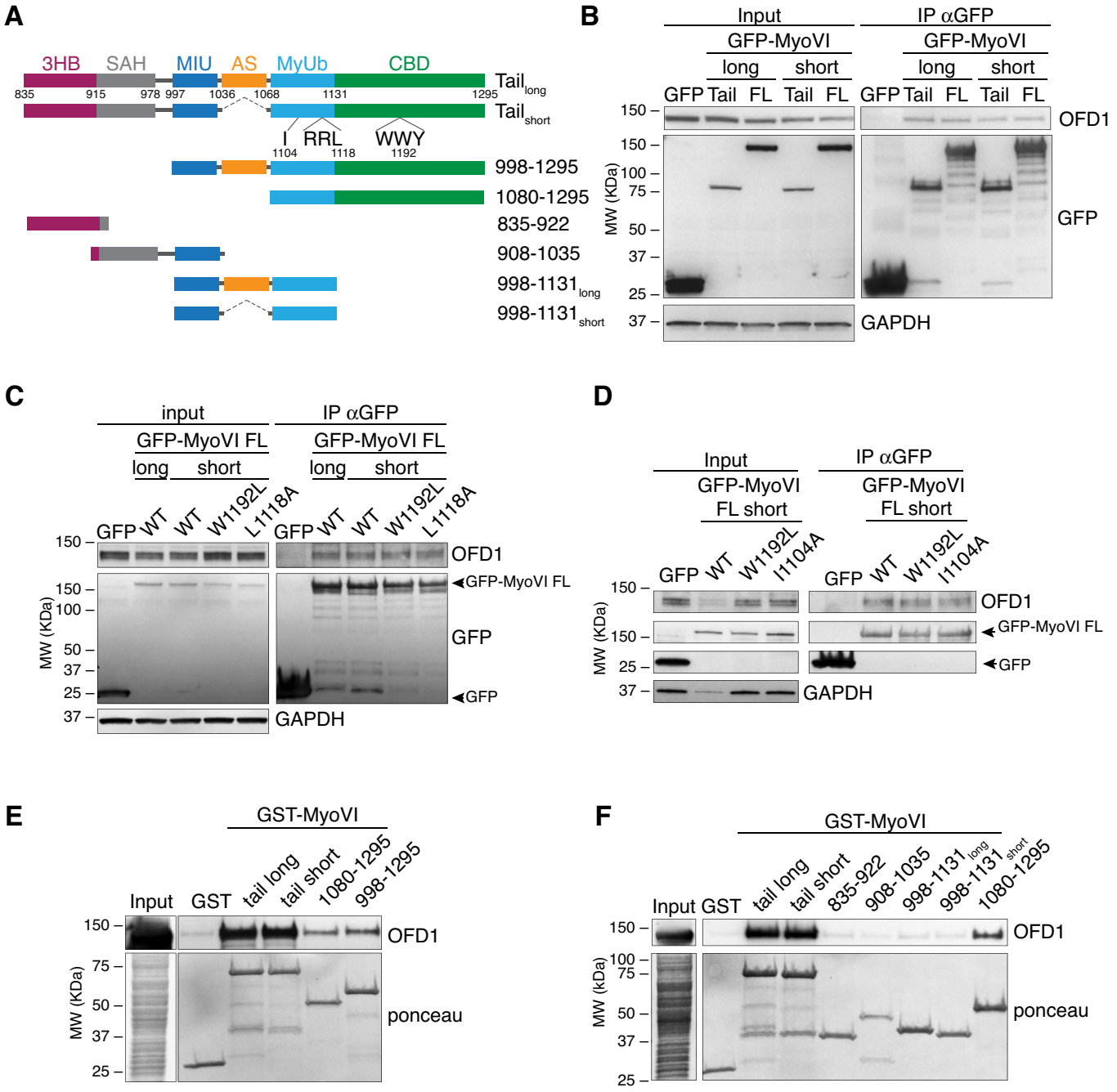

Figure EV2. Characterisation of the myosin VI minimal region of binding to OFD1.

A A scheme of the structure and domain organisation of myosin VI. The tail domain is composed of a three-helix bundle (3HB), a single alpha helix (SAH), two ubiquitin binding regions (MIU, motif interacting with ubiquitin; MyUb, Myosin VI ubiquitin binding domain), and a cargo binding domain (CBD). Between the MIU and the MyUb, an alternative spliced region (AS, in orange) is present in myosin VI$_{long}$ isoform, while it is absent in the myosin VI$_{short}$ isoform. RRL and WLY domains and their single amino acid mutations used in (C, D) are indicated. I1104A affects the Ub binding capacity (He *et al*, 2016), L1118A induces a conformational change that converts a myosin VI long into a myosin VI short-like protein and abrogates binding to GIPC, optineurin and clathrin, while W1192L abrogates binding to Dab2 (Wollscheid *et al*, 2016).

B–D Total lysates from HEK293T transfected with Flag-OFD1 and the indicated GFP-myosin VI constructs were IP with anti-GFP antibody-conjugated beads. IB was performed with anti-OFD1 and anti-GFP antibodies. Anti-GAPDH was used as loading control. FL, full length.

E–F Total lysates from HEK293T cells transfected with Flag-OFD1 were subjected to pull-down assay using the indicated GST-myosin VI constructs or GST alone as control. IB was performed with anti-Flag antibody. Ponceau staining as indicated.

Source data are available online for this figure.

Figure EV3. Myosin VI depletion does not affect centrioles ultrastructure.

A Transmission electron microscopy (TEM) analysis of centriole structure in hTERT-RPE1 control and myosin VI-depleted cells. Representative images are shown, scale bar 500 nm except for the central image that is 200 nm. Centrioles appear morphologically well-organised.

B Depletion of myosin VI leads to displacement of the centrosomes from the cell cortex. hTERT-RPE1 cells were transfected with the indicated siRNA oligos and, after 96 h, were stained with anti-pericentrin to mark centrioles, phalloidin-TRITC to mark cortical actin, and DAPI to mark the nuclei. Left, the distance of the centrosome from the plasma membrane was calculated using ImageJ from XZ-axis images of the cells. Bars represent mean ± SD. $n = 41–45$ cells/condition were counted from three independent experiments. ****$P < 0.0001$ by Kruskal–Wallis test. Centre, representative images are shown; scale bar, 5 μm. Increased distance between centrioles and nuclear membrane in myosin VI-depleted cells is evident. Right, IB analysis showing myosin VI depletion in representative samples.

C Representative images of the samples quantified in B showing myosin VI depletion across the different cell populations. Scale bar, 20 μm.

D Nocodazole treatment leads to the dispersion of OFD1 satellite pool. hTERT-RPE1 cells were treated with nocodazole at 6 μg/ml for 1 h prior fixation to scatter the centriolar satellites and remove OFD1 satellites pool. Cells were immunostained with the anti-OFD1 antibody and the indicated markers for centriolar satellites (anti-PCM1) and centrioles (anti-centrin1). Representative images are shown; Scale bar, 2 μm.

E Effect of nocodazole treatment on GFP-OFD1 localisation in hTERT-RPE cells stably expressing GFP-OFD1 and centrin1-dTomato, used in FRAP experiments shown in Fig 4. Representative images are shown; scale bar, 2 μm.

Source data are available online for this figure.

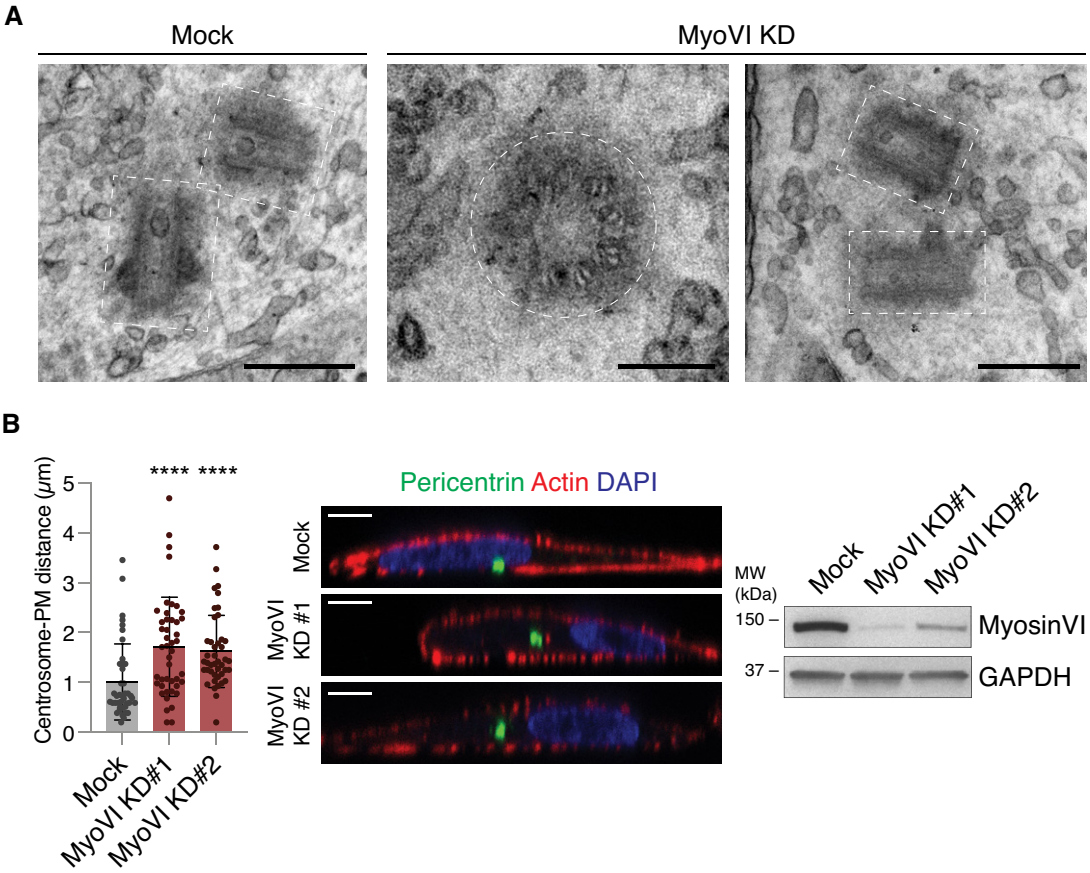

Figure EV3.

Figure EV4. Myosin VI ablation causes p53-dependent cell cycle arrest.

A–C Severe proliferation impairment in myosin VI-depleted RPE1 cells is reproducible using a second siRNA oligo against myosin VI (KD#2). Impairment in cell proliferation was previously shown in rat p53-proficient PC12 cells (Majewski *et al*, 2011). (A) Growth curve of hTERT-RPE1 cells transfected with a second myosin VI siRNA oligo +/− p53 siRNA oligo. A representative plot of three independent experiments is shown. (B) Representative bright-field images of cells treated with the indicated p53 and myosin VI siRNAs. Scale bar 200 nm. (C) IB analysis of control and myosin VI-depleted hTERT-RPE cells with anti-myosin VI, anti-p53 and anti-p21 antibodies.

D–F Myosin VI depletion does not affect cell proliferation in p53-null tumour cells. (D) Growth curve of hTERT-RPE1, HeLa and Caco-2 cells transfected with myosin VI siRNA measured by Incucyte. A representative plot of two independent experiments is shown. Data are reported as mean ± SD of three technical replicates. (E) Cell viability of the indicated cell lines measured by crystal violet staining. (F) IB analysis of the indicated cells lines, control and myosin VI-depleted, with anti-myosin VI, anti-p53 and anti-p21 antibodies. Anti-GAPDH was used as loading control.

Source data are available online for this figure.

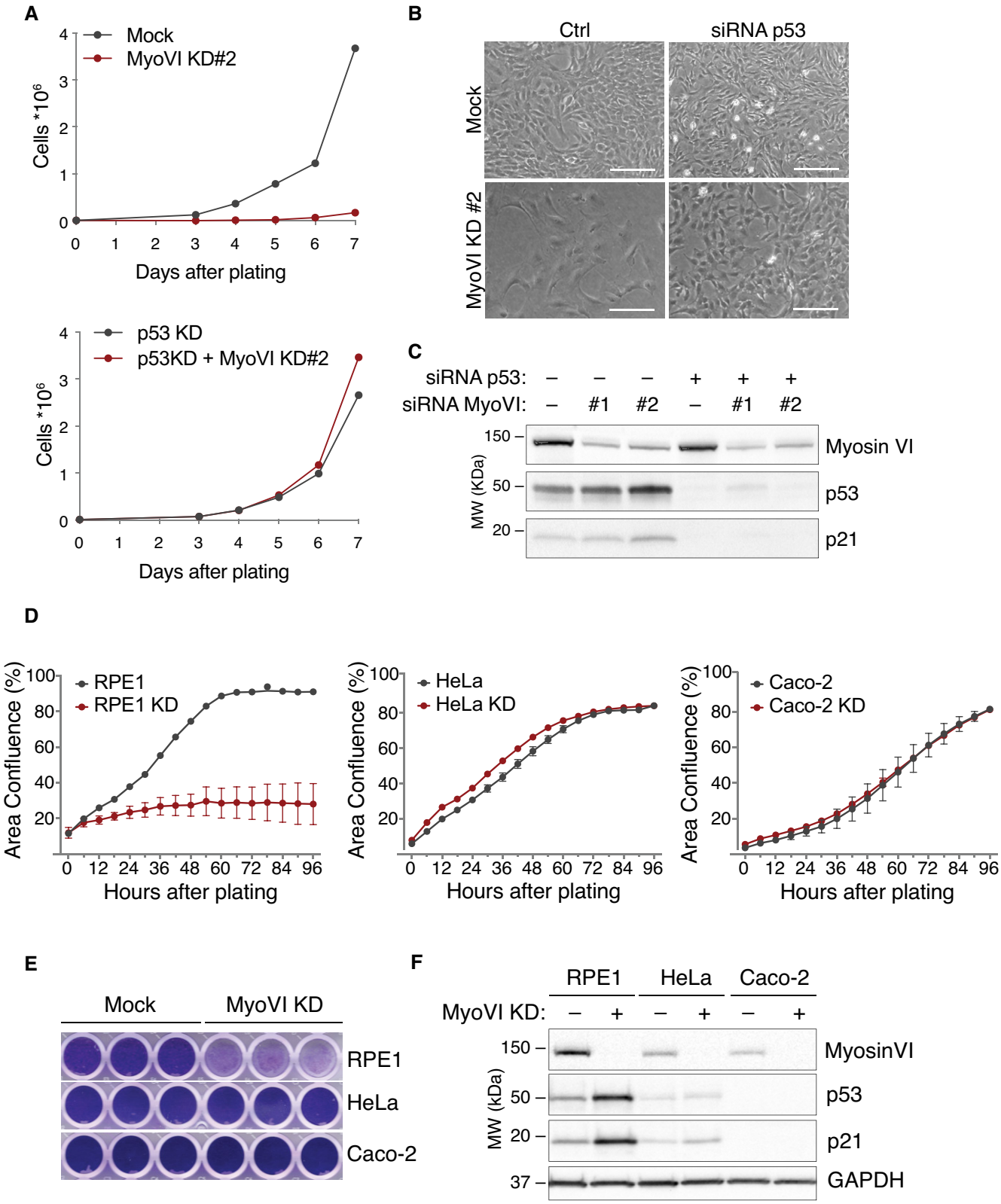

Figure EV4.

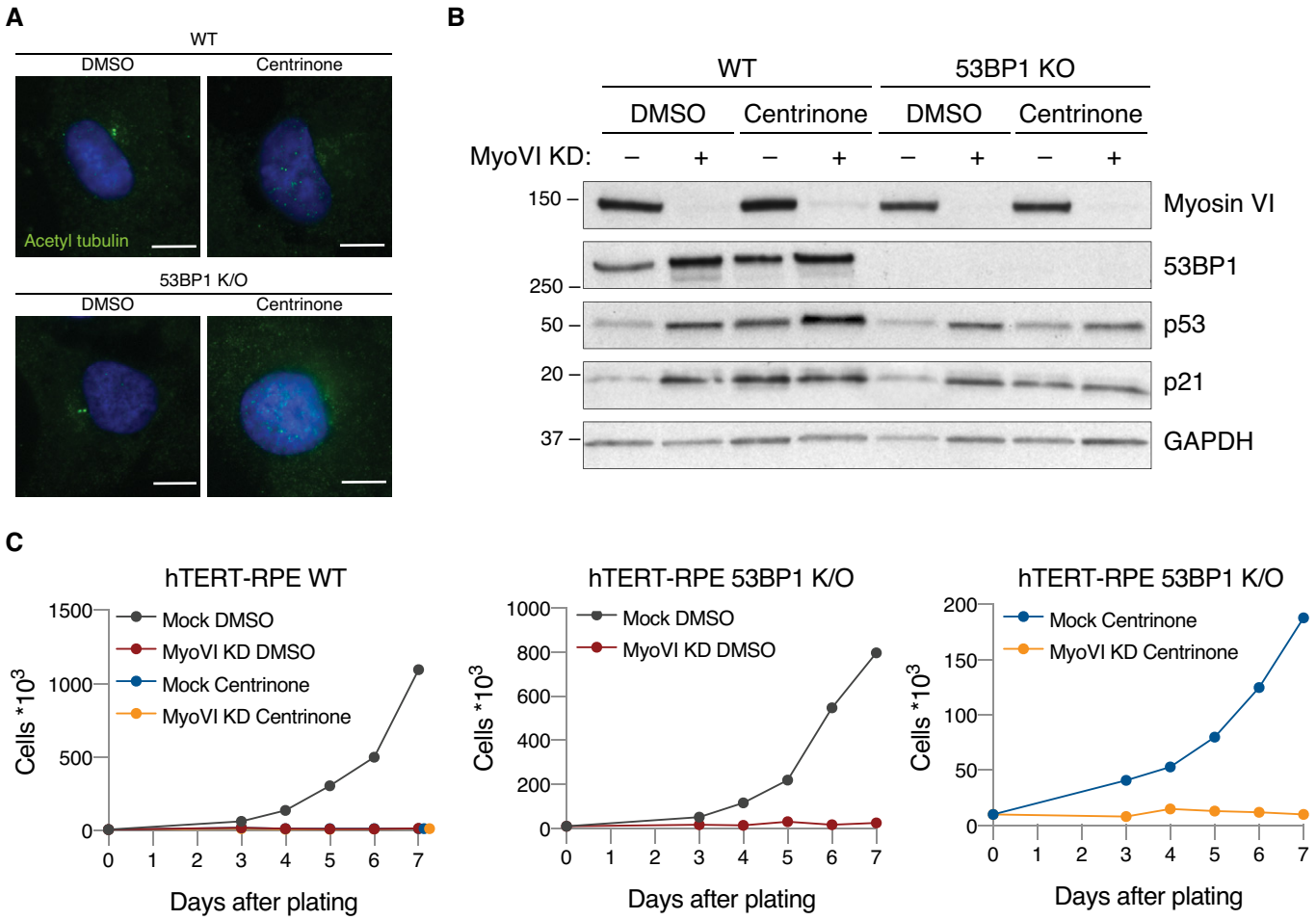

Figure EV5. p53 activation in myosin VI-depleted cells is not due to its effect on centrioles.

In centrinone-treated 53BP1 KO cells, myosin VI depletion caused p53 activation and cell cycle arrest similar to wild-type cells.

A hTERT-RPE1 wild-type or 53BP1 KO cells were treated with centrinone or DMSO and immunostained with anti-acetylated tubulin antibody and DAPI to verify the presence or absence of centrioles. Representative images are shown, scale bar, 20 μm.

B IB analysis of hTERT-RPE wild-type or 53BP1 KO cells transfected with myosin VI siRNA and treated as indicated. Anti-GAPDH was used as loading control.

C Growth curves of hTERT-RPE1 wild-type or 53BP1 KO cells transfected with myosin VI siRNA and treated as indicated. Representative plots of three independent experiments are shown.

Source data are available online for this figure.